NSW Natural Resources Commission

Forest Monitoring and Improvement Program:

Foundational Priority Projects

Supporting post-fire ecological resilience and recovery planning in NSW forests

Milestone 2

Progress Report - October 2020

Rebecca Gibson[1], Anthea Mitchell[2,3],
Jim Watson[2,4], Adrian Fisher[3,2], Sam Hislop[5], Tim Danaher[1,2]

[1]Department of Planning, Industry and Environment (DPIE)

[2]Joint Remote Sensing Research Program (JRSRP)

[3] University of NSW (UNSW)

[4]The University of Queensland (UQ)

[5]Deparment of Primary Industries, Forestry

Citation:

Gibson, R.K, Mitchell, A., Watson, Fisher, A., J., Hislop, S., Danaher, T. (2020) Supporting post-fire ecological resilience and recovery planning in NSW forests, Milestone 2 Progress Report, Natural Resources Commission Forest Monitoring and Improvements Program, https://www.nrc.nsw.gov.au/fmip

Contents

1. Summary of Progress

Remote sensing approach to monitoring post-fire vegetative recovery

The project aims to develop new remote sensing tools for forest managers to undertake risk assessments and subsequently plan and report on post-fire ecological recovery. A key component of our research is to develop a method that measures the proportion of vegetative regrowth relative to the unburnt or pre-fire state, with the view to possible integration with the DPIE-RFS semi-automated fire severity mapping system (FESM). These data products would be aimed at suiting an ongoing monitoring framework and would provide post-fire recovery data over longer timescales. Our work so far has focused on how best to define the pre-fire state and developing programming code to allow repeatable rapid processing and analysis of candidate recovery indices. Our exploration of candidate indices will continue as field data is captured for quantitative comparisons.

Fire severity derived products - unburnt refugia

In order to support land managers in post-fire recovery decisions and prioritisation of resources immediately following fire events, we have also been developing a set of example decision support products derived from FESM severity maps. In the past few months, we've harnessed an opportunity to work closely with NPWS executives, to build and deliver a proof of concept case study of historical fire severity and derived spatial products, as well as statistical analyses to help inform recovery planning and potential indicators of ecological resilience. The work focused on building the historical severity mapping archive for the Blue Mountains and subsequently analysing landscape patterns in short-term and long-term unburnt refugia. Preliminary results are provided here, but we look forward to continuing collaborations with senior NPWS managers to improve the post-fire recovery decision support products and applications.

TLS acquisition

In August 2020, the DPIE Remote Sensing and Regulatory Mapping team acquired a terrestrial laser scanner. The TLS instrument will provide high density point clouds to generate high resolution 3D images of forest structure and biomass. This will provide a valuable contribution of quantitative field measurements and allow for high precision repeated measures across time. We have leveraged significant in-house expertise through the joint remote sensing research program, particularly with our research partner Dr Nick Goodwin, in developing data management protocols and automated workflows for file naming conventions, data storage, pre- and post-processing and analysis. We have adapted our fieldwork plans for this project to extensively use the TLS, as this will provide field data of far greater precision and quality than our previously proposed field methods. The investment in building our TLS data capture, management and processing protocols will provide enduring benefits for this project.

Scheduled Fieldwork Delays

Since our project's inception in October 2019, we have experienced the unprecedented 2019/20 summer bushfire crisis which put considerable demand on the project lead, Rebecca Gibson, due to DPIE corporate requirements for rapid response severity mapping (FESM). The bushfire crisis was closely followed by the COVID-19 pandemic which saw DPIE offices closed as we were required to work from home from April 2020. Field work restrictions have now eased to allow approval of field trips where necessary for critical business. New DPIE COVID-safe protocols for fieldwork restrict passengers in a vehicle to a maximum of 2. In some cases, the demand for departmental vehicles out-strips supply, causing logistical difficulties. Despite the challenging circumstances, we have made progress with field work and will continue to focus on setting up sites for repeated measures, to ensure 2 to 3 site revisits can be accomplished before November 2021.

2. Landsat historical severity mapping - algorithm development and testing

Background

Building the historical severity archive to retrospectively map past fires using Landsat imagery has been part of the long-term goals of the FESM project. The first step toward this outcome was to modify and test the original Sentinel 2 based algorithm to suit Landsat satellite imagery. Here we present the results of this work, with comparison of performance between the algorithms. This work has been essential in supporting the research for the post-fire recovery project, to allow severity mapping of historical fires as the starting point in assessing methods of monitoring long-term post-fire recovery.

Method

In developing the original Sentinel 2 FESM algorithm, we considered future application onto Landsat imagery was likely. As such, the Sentinel 2 input imagery was pre-processed into a 'Landsat TM - like' configuration to allow for backward compatibility with Landsat. However, preliminary attempts to apply the Sentinel 2 algorithm directly onto Landsat imagery without modification had limited success. Sentinel 2 differs slightly in the configuration of bandwidths compared to Landsat OLI (Landsat 8). Likewise, Landsat OLI differs slightly in bandwidths compared to Landsat TM (Landsat 5 and 7). There was enough difference between these sensors to produce noisy output in the random forest supervised classification, producing low prediction accuracy. Therefore, the algorithm has been modified and trained separately to suit each specific sensor.

See Gibson et al (2020) for further details on the method of FESM supervised classification using a random forest machine learning framework. The severity classification definition is provided here (**Table *1***).

Table 1 FESM severity class definitions

Severity class	Description	% foliage fire affected
Unburnt	Unburnt understory and unburnt canopy	0% canopy and understory burnt
Low	Burnt understory with unburnt canopy	>10% burnt understory >90% green canopy
Moderate	Partial canopy scorch	20-90% canopy scorch
High	Full canopy scorch (+/- partial canopy consumption)	>90% canopy scorched <50% canopy biomass consumed
Extreme	Full canopy consumption	>50% canopy biomass consumed

Results

High resolution aerial photographs were used to develop the severity class training samples, which were then used for extracting the spectral information from the satellite imagery to train the supervised classification, specific to each different sensor. Due to the different mission date ranges of the satellites, some fires training data have been able to be used in multiple sensor-specific algorithms (**Table *2***).

Table 2 Fires and corresponding aerial photography used to train sensor-specific algorithms for supervised classification of fire severity.

Fire name	Fire start date	Aerial photo date	Aerial photo resolution (cm)	Training data used for sensor-specific algorithm		
				Sentinel 2	Landsat OLI 8	Landsat TM 5 and 7
Sir Ivan	20170217	201702	50	yes	yes	no
White Cedars	20170212	201702	20	yes	yes	no
Wollemi 695	20180128	201803	50	yes	yes	yes
Mt Canobolas	20180210	201803	30	yes	yes	no
Sir Bertram	20180120	201803	50	yes	yes	no
Pilliga	20180119	201803	50	yes	yes	yes
Tathra	20180318	201803	10	yes	yes	yes
Holsworthy	20180413	201804	50	yes	yes	no
Port Stephens	20131013	201310	10	no	no	yes
Springwood	20131017	201310	10	no	no	yes
Wambelong	20130112	201301	50	no	no	yes
Wyong	20131017	201310	10	no	no	yes
Yarrabin	20130106	201301	20	no	no	yes

Table 3 Averaged Balanced Accuracy and Kappa statistics

FESM class	FESMv2 Sen2	FESMv2 L8
Unburnt	0.975	0.959
Low	0.827	0.861
Moderate	0.655	0.669
High	0.836	0.787
Extreme	0.909	0.895
Kappa	0.718	0.709
Overall accuracy	0.80	0.82

The same set of 8 case study fires were used to train both the Landsat OLI and Sentinel 2 algorithms. These cases have been used in a systematic cross-validation analysis to compare the algorithm performance between sensors, provided in appendix Table 13 **Balanced Accuracy and Kappa statistics for predictive models for each fire.**Table 13, with the averaged results in **Table *3***. The results indicate comparable accuracy across fire severity classes between Sentinel 2 and Landsat 8 sensor-specific algorithms. Both models have kappa scores above 0.70, indicating equally robust overall performance. Extensive interpretation of the severity maps generated by alternative sensor-specific algorithms have also been assessed against high resolution post-fire aerial photography (see Figure 1). In some cases, the larger pixel size of Landsat compared to Sentinel 2 pixels (30m vs 10m) slightly improved the classification of low severity under sparse canopy, for example in the Pilliga. This key finding will be further considered in future revision of texture metrics of the Sentinel 2 algorithm. The FESM operational system has been updated to accommodate the different sensor platforms with automated application of each appropriate training dataset.

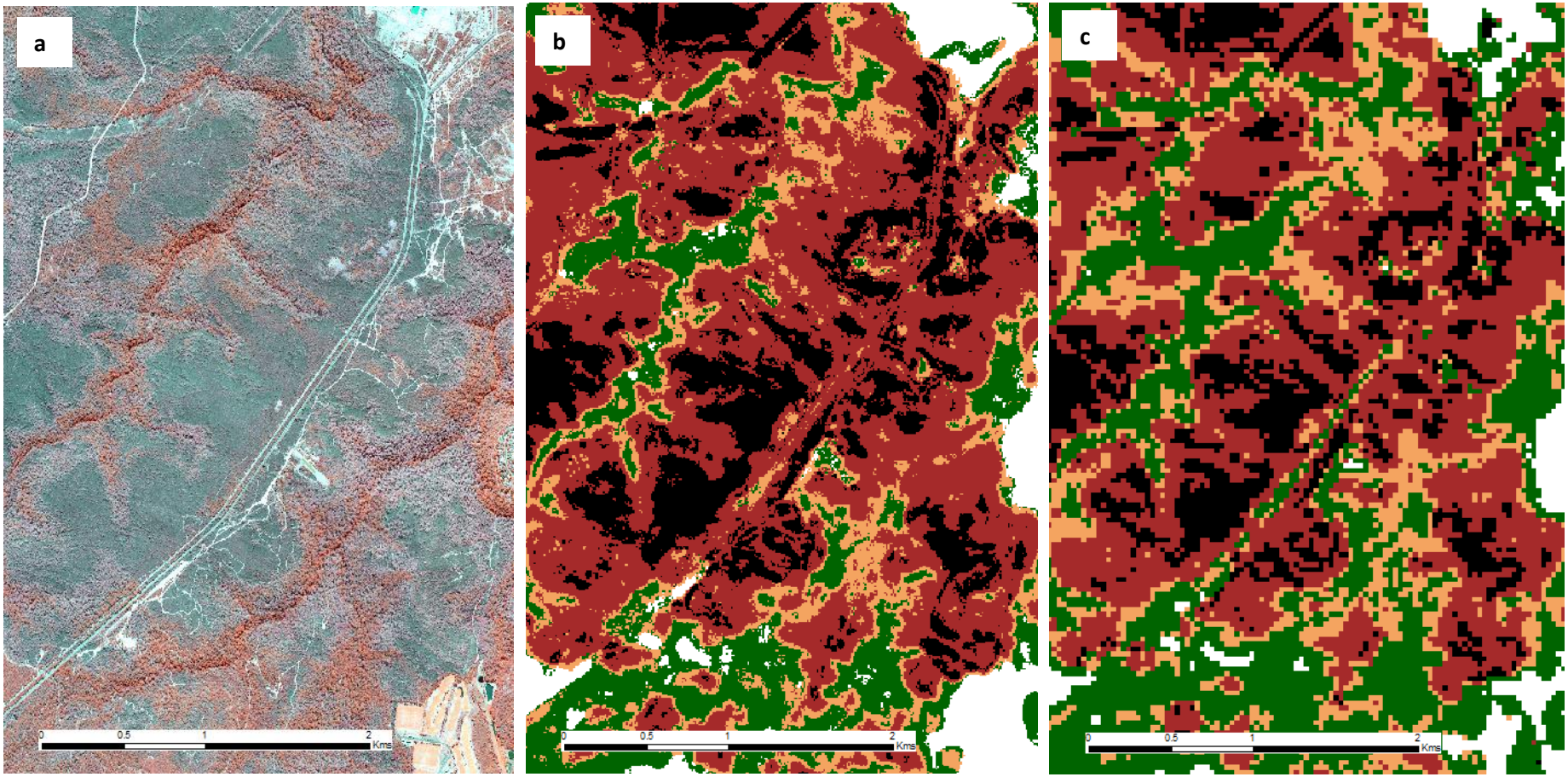

Figure 1 Visual comparison of high-resolution post-fire aerial photography (a), sentinel 2 (b) and Landsat 8 (c) sensor-specific severity classifications

3. New tools for risk assessment and post-fire ecological recovery planning

Background

We have recently been involved in a package of work at the request of the NPWS Deputy Secretary and senior management for a rapid assessment of the effects of fire on reserves within the Blue Mountains area, with a view to informing appropriate indicators used to measure 'ecological health' (perhaps better defined and quantified as ecological resilience). Although this case study was not in the original scope of work for this research project, the objectives closely align so the time investment was considered mutually beneficial and complementary. Directly working with senior land managers to craft fit-for-purpose tools derived from remote sensing of fire is a major benefit to the outcomes of our project.

Existing indicators of effects of fire focus on fire frequency, time since last fire and inter-fire interval as a measure of whether the fire regime is appropriate for the ecosystem. The measurement of other variables such as severity and patchiness may provide improved understanding of the impacts and response of flora, fauna and ecosystems to fire. Unburnt patches within a fire extent may act as refugia, facilitating survival and persistence of species. However, patchiness and edge effects may have contrasting values depending on the ecological context. For example, high edge density (i.e. high patchiness of unburnt refugia) may increase habitat suitability for some animal species (e.g. it may increase their ability to use and/or recolonise burnt areas). In contrast, high edge density can increase predation rates, depending on the species.

There is uncertainty about the appropriate scale at which unburnt mosaics should be maintained, and this will vary between ecosystems. Furthermore, it is unlikely that the unburnt patch configuration resulting from a single fire event will provide robust information about ecological resilience. However, long unburnt refugia over 10, 20 and 30 years may provide more significant insights.

Method

Fire severity derived products - unburnt refugia

The first major component of this case study was to map historical severity for the Blue Mountains study area. The previously completed work in adapting the sentinel 2 FESM algorithm for application on Landsat imagery was the prerequisite that allowed the Blue Mountains archive from 1989 to 2020 to be mapped. Fire year mosaics were produced by compositing the individual severity maps in each fire year. A binary reclassification of the FESM severity classes was made to represent burnt canopy and unburnt canopy (see **Table *4***, ***Figure 2***). Using the burnt canopy fire year mosaics, time since canopy fire and canopy fire frequency products were subsequently generated.

Table 4 Class definitions and relationship between FESM severity classes and the burnt canopy binary reclassified product.

FESM			**Burnt Canopy Binary Reclassification**		
Label	**Description**	**Pixel value**	**Label**	**Pixel value**	**Description**
Unburnt	Unburnt understory with unburnt canopy	0	Canopy unburnt	0	Unburnt or low severity
Low	Burnt understory with unburnt canopy	2			
Moderate	Partial canopy scorch	3	Canopy burnt	1	All canopy level fire combined, from partial scorch to full consumption
High	Full canopy scorch	4			
Extreme	Full canopy consumption	5			

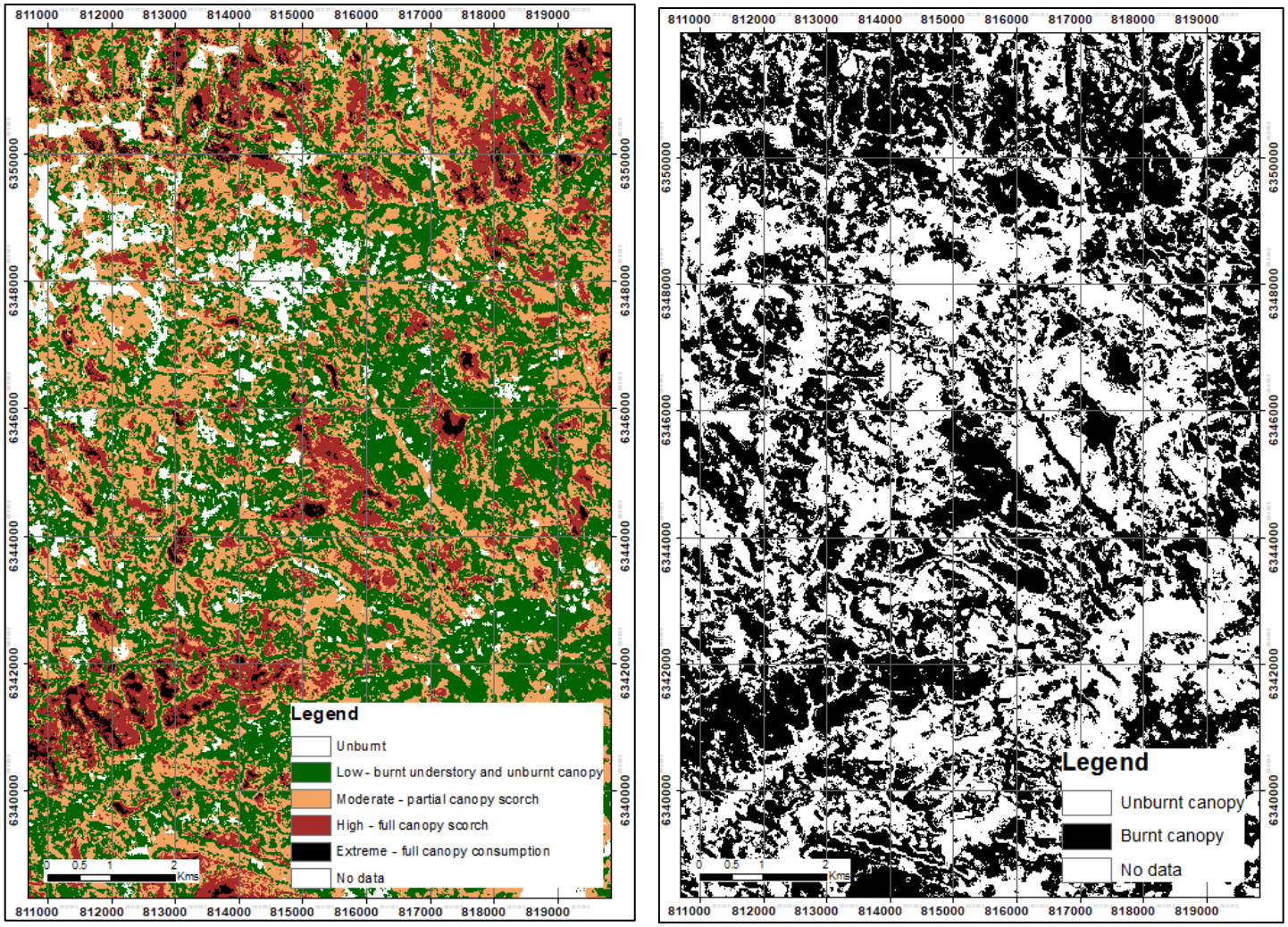

Figure 2 Comparison of a single location mapped by the FESM severity classes (a) and the burnt canopy binary reclassified product (b).

Results

Landscape pattern analysis of patch metrics

Landscape ecology research tools are well established in the literature and available for quantitative, spatial analysis of landscape patterns such as habitat fragmentation. Fragmentation statistics have been widely used in the literature, with standard formulas implemented in various software library packages, including R ('landscapemetrics') and python ('PyLandStats') as well as standalone opensource software ('FRAGSTATS').

For the Blue Mountains rapid assessment case study, I used FRAGSTATS calculated by NPWS Estate for relative comparisons. For demonstration of the concept and potential applications, I selected a set of standardized metrics to allow comparisons among landscapes with different total areas, with simple, intuitive interpretations (**Table *5***) and applied them to each NPWS estate for the 2019/20 fire year (**Figure *3***) as well as for the 10, 20 and 30 year fire frequency composites (not presented here).

Table 5 A selection of FRAGSTAT metrics used in the Blue Mountains case study.

FRAGSTAT metric	Definition	Behaviour of statistic
Proportion of landscape	Area in hectares of class *i* (i.e. unburnt canopy)	Simple absolute measure
Patch density (n/100ha)	Number of patches of class *i* per 100 hectares.	Increases as the landscape gets more patchy.
Edge density (m/ha)	the sum of all edges of class *i*	Increases as the landscape gets more patchy.
Distance between patches (coefficient of variation in Euclidean nearest neighbour distance)	The ratio of the standard deviation to the mean (a dimensionless number). Euclidean geometry is the shortest straight-line distance between the focal patch and its nearest neighbour of the same class.	Approaches 0 as distance decreases, i.e. patches are more aggregated. Increases as distance between patches increases, i.e. patches are more isolated.

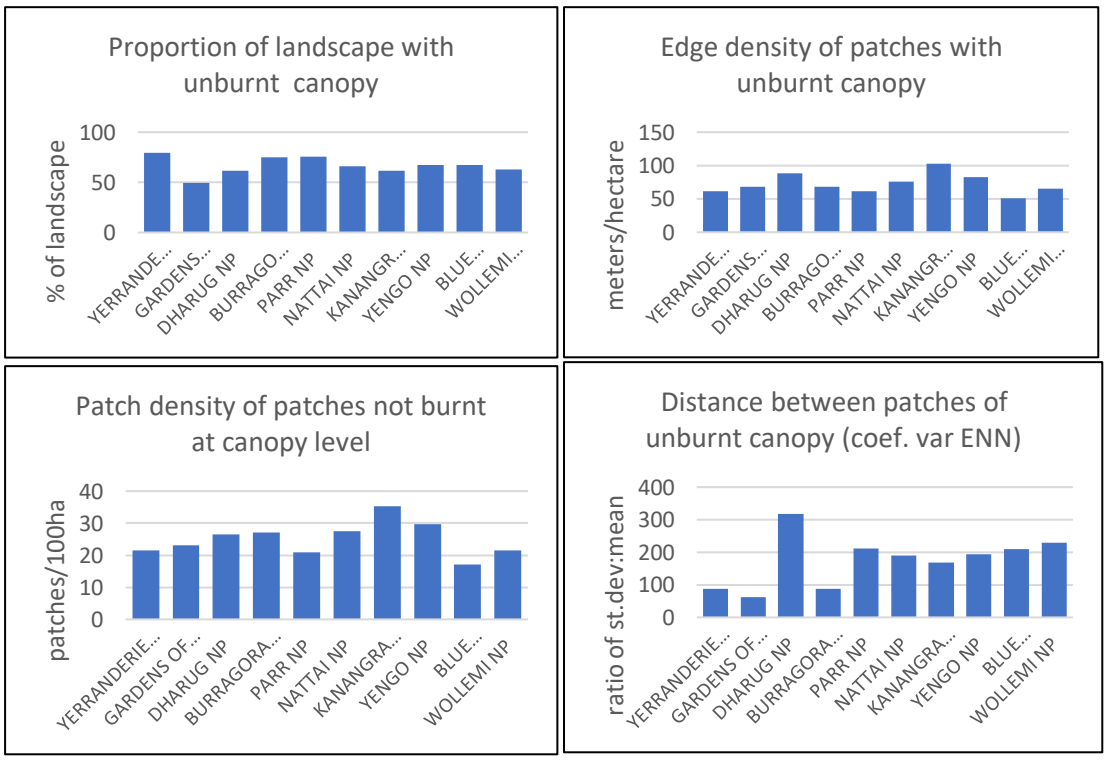

Figure 3 FRAGSTAT metrics used, applied to each NPWS reserve for the 2019/20 fire assessment in the Blue Mountains case study.

Interpretation and further refinements

The results so far demonstrate the application of fragmentation statistics for understanding landscape patterns in unburnt patch configuration following a single fire, as well as long unburnt refugia across several decades of fire impacts. However, the interpretation of how these metrics contribute to understanding the impacts and response of flora, fauna and ecosystems to fire is less clear. While comparisons between reserves may assist in resourcing decisions, the suitability of these landscape metrics for conservation management decisions requires further refinements to provide an ecological context to support conservation management decisions at the landscape scale.

Further work is planned for the next few months to address minor data quality refinements (to add fire start date details for missing fires in the historical archive) and reprocess finalised file formats of the fire year mosaics, fire frequency and TSF products. Then we will provide some improved ecological context by intersect unburnt canopy products with vegetation formation and topographic position (i.e. ridge, gully, slope) and re-running the landscape pattern statistical analyses. Further integration of this research into our broader post-fire recovery monitoring framework will aim to provide quantitative evidence and further understanding of the effect of unburnt canopy patchiness on ecological resilience.

4. Exploration of candidate spectral recovery indices and techniques

Background

One of the key objectives of our project is to develop a remote sensing method that estimates the proportion of vegetative regrowth since a forest fire event relative to the unburnt or pre-fire state, at regular post-fire intervals to support a monitoring and reporting framework. In exploring reflectance indices from passive optical sensors, post-fire recovery rates will represent the change in reflectance values of the upper-most vegetation layer, without attempting to separate canopy from sub-canopy components. This is often assumed to represent the tree canopy but may involve a mixture of reflectance signal from canopy and sub-canopy components, depending on the structural composition and canopy density.

A wide range of previous literature exists on the performance of various spectral vegetation indices in remote sensing post-fire recovery studies. The commonly used normalised burn ratio (NBR) index is a ratio of the near infra-red (NIR) to a shortwave infrared (SWIR) band. This index has been demonstrated to have greater sensitivity to finer changes in vegetation cover after disturbance over longer recovery timeframes compared to other common vegetation indices such as NDVI. A modification of the traditional NBR index has also been developed to compare the two SWIR bands instead of the NIR, known as NBR2, and appears to fluctuate less with annual variation in vegetation and soil moisture and represents longer term recovery trends than NBR (Hislop et al 2018; **Table *6***).

Spectral indices are unitless values that do not directly measure any biophysical property. As such, indices measuring the relative cover of photosynthetic, non-photosynthetic material and bare ground (i.e. sub-pixel unmixing models) may provide a more appropriate remote sensing surrogate to estimate the change in biomass due to fire compared to traditional reflectance-based estimates. Although not widely applied in post-fire recovery studies, this may be due to data availability and the complexity of building a robust sub-pixel unmixing model using widespread and high-quality field calibration data. In the preliminary exploration of spectral recovery indices and techniques, we have initially focused on NBR and fractional cover-based indices. This does not preclude other reflectance-based index options we may still examine.

In estimating a measure of ecological resilience, a critical component of the methodology is defining the pre-fire state to assess the magnitude of perturbation and rate of recovery back to the pre-fire baseline. There is added complexity in defining the pre-fire baseline within a rapidly changing climate. For example, altered seed bank dynamics and reduced growth rates with increased fire frequency and declining moisture availability may slow forest recovery or prevent the complete recovery of forest height and structure to the pre-fire state. Therefore, defining an alternative stable state may be required. Another methodological challenge will be taking account of subsequent disturbance prior to full recovery, which is likely to become more common as fire frequency is projected to increase in the future.

Another key challenge when using multitemporal imagery to monitor vegetation change is to identify the relevant features of a time series while dismissing noise introduced by ephemeral changes in illumination, phenology, atmospheric condition and geometric registration. Calibration data from unburnt reference pixels that are monitored alongside the fire affected area can be used effectively as a phenological offset, to control for sources of noise and better represent the change due to post-fire recovery. Here we summarise our preliminary exploration of contrasting methods to define the pre-fire state and the effect of applying an unburnt reference calibration.

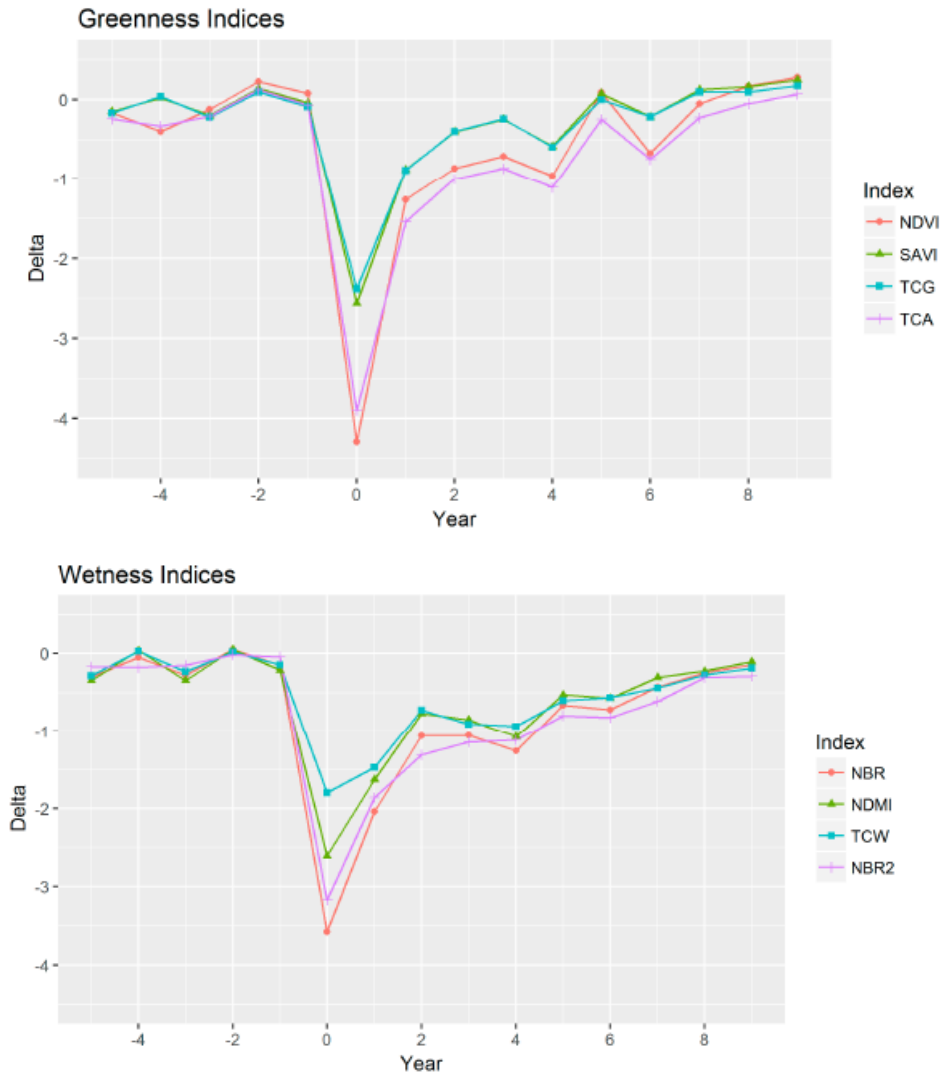

Table 6 Mean values for common greenness and wetness indices from five years prior to fire to nine years post-fire (Hislop et al 2018), including NDVI (normalised differenced vegetation index), SAVI (soil adjusted vegetation index), TCG (Tasselled Cap Greenness), TCA (Tasselled Cap Angle), NBR (normalised burn ratio), NDMI (normalised differenced moisture index), TCW (Tasselled Cap Wetness) and NBR2.

Preliminary Method and Results

Candidate indices

We examined the variation in NBR and fractional cover values for imagery across several years before and after a fire event, within the prism of different severity classes. Data from one fire presented here, White Cedars in 2017, demonstrates the consistent pattern observed at a wide range of other case study fires. Inter-annual variation in rainfall and temperatures cause fluctuations in the NBR and fractional cover values, with a notable drop in NBR and green fractional cover and a corresponding increase in dry and bare cover just after July 2016, which was the start of significant drought conditions in the central west. This was shortly followed by a similar pattern seen in early 2017, just prior to the fire start date (**Figure *4*** and **Figure *5***).

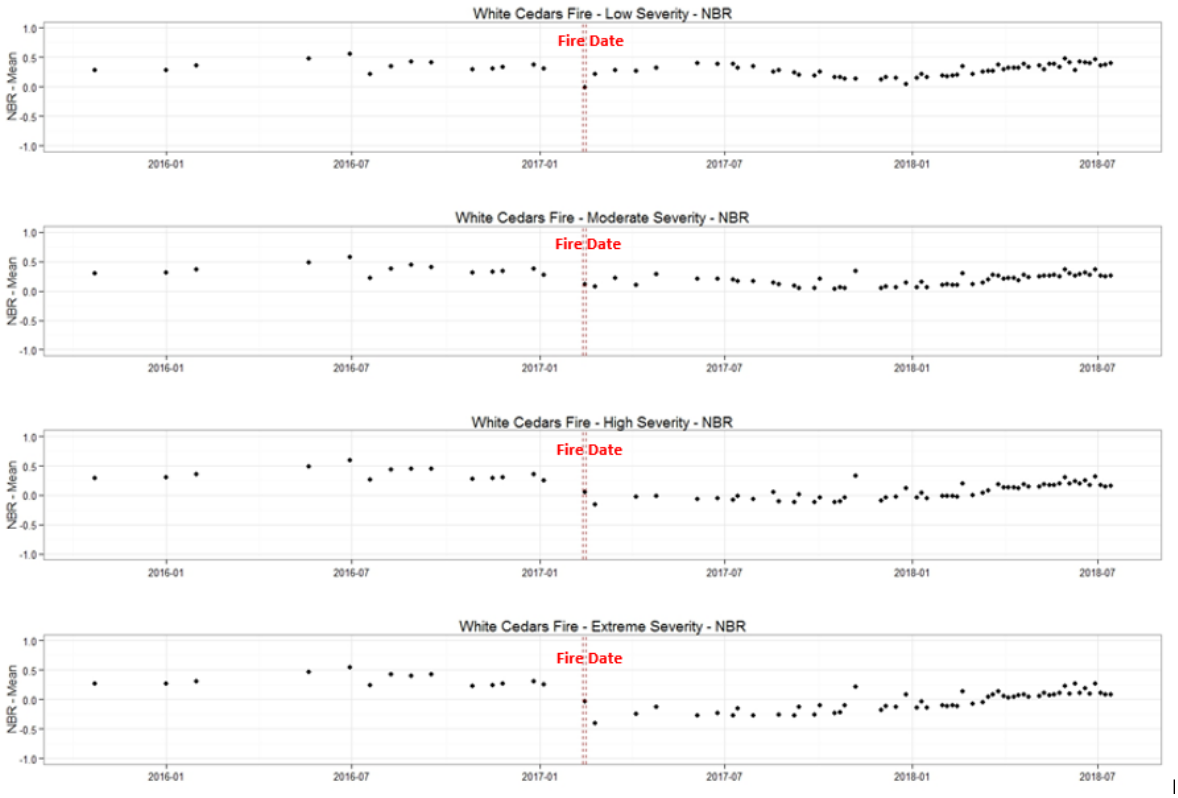

Figure 4 Example of the variation in NBR timeseries pre and post-fire.

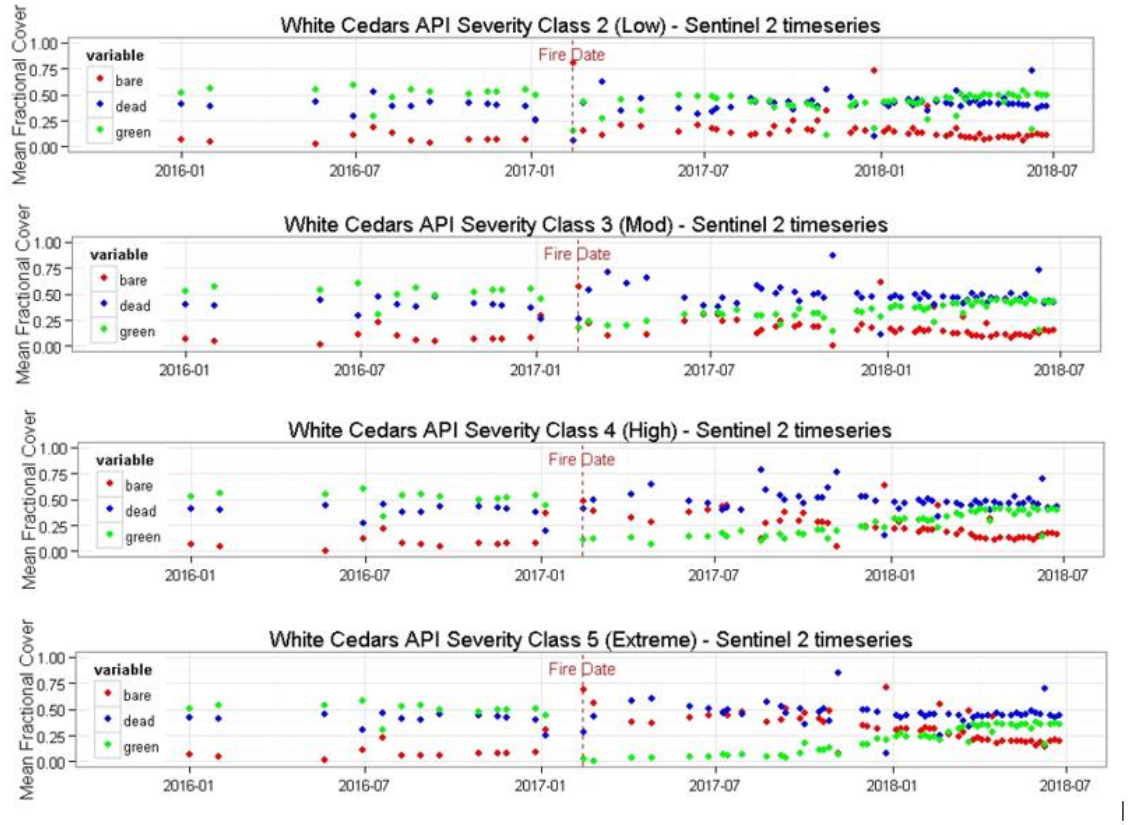

Figure 5 Example of the variation in fractional cover timeseries pre and post-fire, for bare, dead (non-photosynthetic) and green (photosynthetic) fractions.

Pre-fire state definitions

We examined the effects of 2 contrasting methods of defining the pre-fire state. The first method uses a dense stack timeseries statistics tool, 'ffract' developed by Dr Jim Watson, and compares the medoid seasonal fractional cover for a selected statistic (e.g. mean, max, standard deviation, coefficient of variation and others) of the 2 years preceding the fire to the 1 year preceding the target year of assessment. Medoid is similar to mean but is the value that has minimal average dissimilarity from all object in the cluster and is robust to outliers, thereby reducing noise and variance. For a post-fire monitoring tool to assess vegetative recovery at given time-steps, using a statistic such as the mean across an entire year preceding the target year of assessment may reduce the sensitivity of the method to detect finer scale changes on shorter timeframes.

Given this potential limitation, an alternative approach was investigated, based on the selection of 4 cloud free images restricted to the season the fire occurred in. The pre-fire state was calculated as the average of 4 images from the preceding 2 years, in the season the fire occurred in, and 4 images in the season the fire occurred for the target year of assessment.

In both methods, the Relative Recovery Index (RRI) is a pixel-wise calculation of the change between pre and post-fire, relativised to the pre-fire pixel, where a value of 0 indicates no change compared to the pre-fire baseline; positive values indicate an increase in the index value relative to the pre-fire state, and negative values indicate a decline in the index value relative to the pre-fire state:

$$RRI = \frac{(post\text{-}fire - pre\text{-}fire)}{pre\text{-}fire} \quad (1)$$

To demonstrate the preliminary assessment, presented here is the results for 1, 2 and 5 years post-fire for the Warrumbungles fire in 2013, grouped by fire severity class; low (burnt understory, unburnt canopy), moderate (partial canopy scorch), high (full canopy scorch) and extreme (full canopy consumption) for the 'ffract' timeseries (Figure 6) and the 4 image average methods (**Figure *7***).

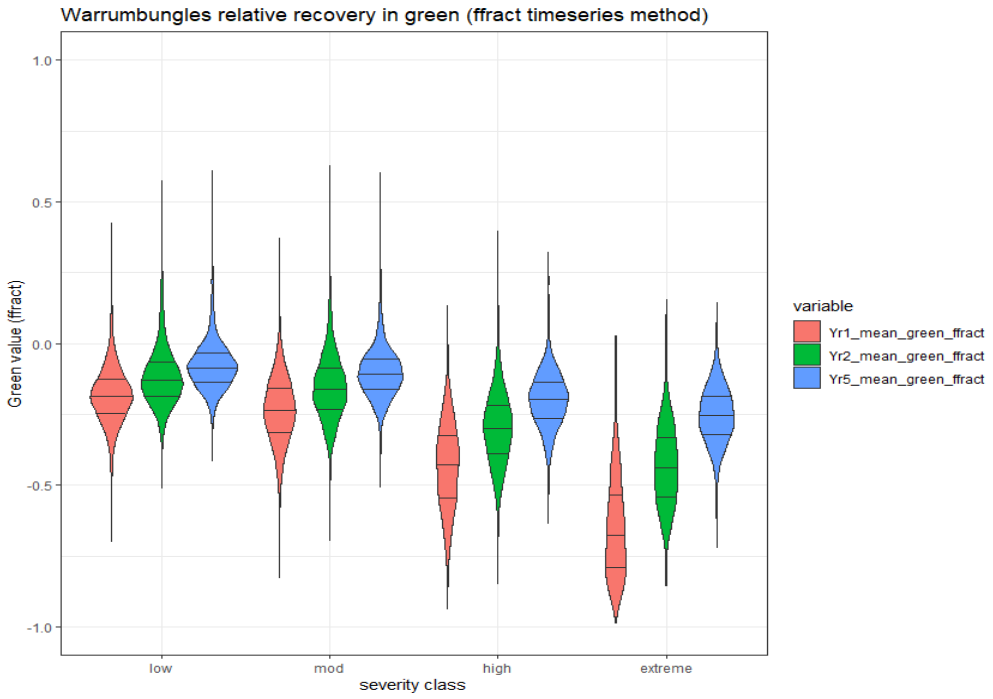

Figure 6 Relative recovery index using the ffract method for 1-, 2- and 5-years post-fire by fire severity class. The violin density plots show the distribution of the data, with 25%, 50% and 75% quantile lines.

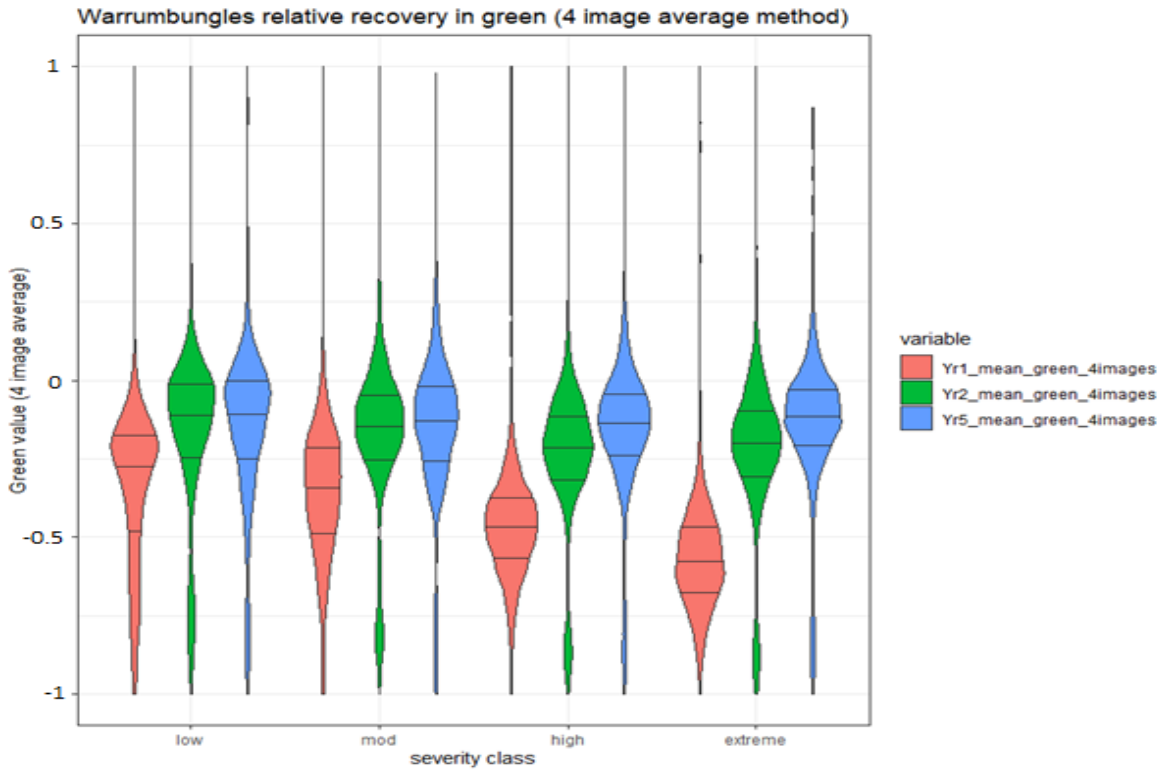

Figure 7 Relative recovery index using the 4-image average method for 1-, 2- and 5-years post-fire by fire severity class. The violin density plots show the distribution of the data, with 25%, 50% and 75% quantile lines.

The effect of fire severity on the Relative Recovery Index is consistent and logical between the two methods, and across time-steps, whereby the higher severity classes had larger post-fire declines in mean green values (or increase in the case of bare fraction, not shown here). In each severity class, there was an incremental return towards the pre-fire baseline (i.e. 0), with larger inter-annual differences for the higher severity classes compared to the lower severity classes.

The preliminary results suggest the much larger volume of images, and the medoid used to calculate the 'ffract' timeseries statistic may the reduce noise and variance observed in the 4-image average method. We will continue to explore different configurations of these methods, for example, the effect of using the dense stack timeseries to define the pre-fire state, compared to the post-fire average of 4 images taken in the season the fire occurred for the target year of assessment, and taking the medoid rather than mean of the 4 images.

Unburnt reference calibration

Unburnt reference calibration may be used in remote sensing of vegetation change to reduce noise and variation due to phenological and seasonal effects. For example, a phenological offset of unburnt training data is incorporated into the automated processing workflow of the FESM system. Using the ffract timeseries and the 4 image average methods, we generated the Relative Recovery Index for the same unburnt reference area used in the FESM model to capture unburnt training data. In all years, there was considerably higher variation in the 4-image average method, compared to the ffract method. However, both methods show that all years had a lower mean green value in the unburnt reference relative to the pre-fire state, with year 1 having a relatively greater decline.

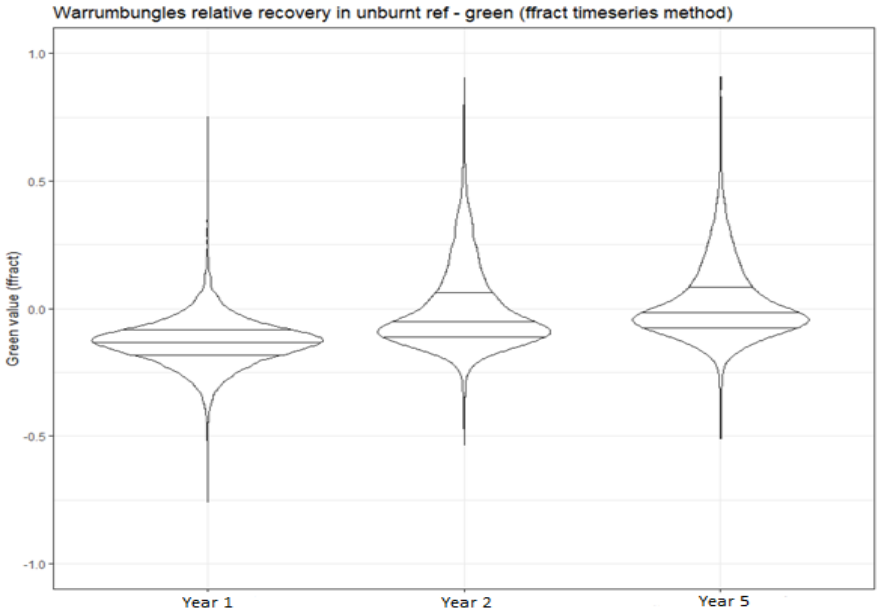

Figure 8 Relative recovery index for mean green fraction in the unburnt reference using the 'ffract' timeseries method

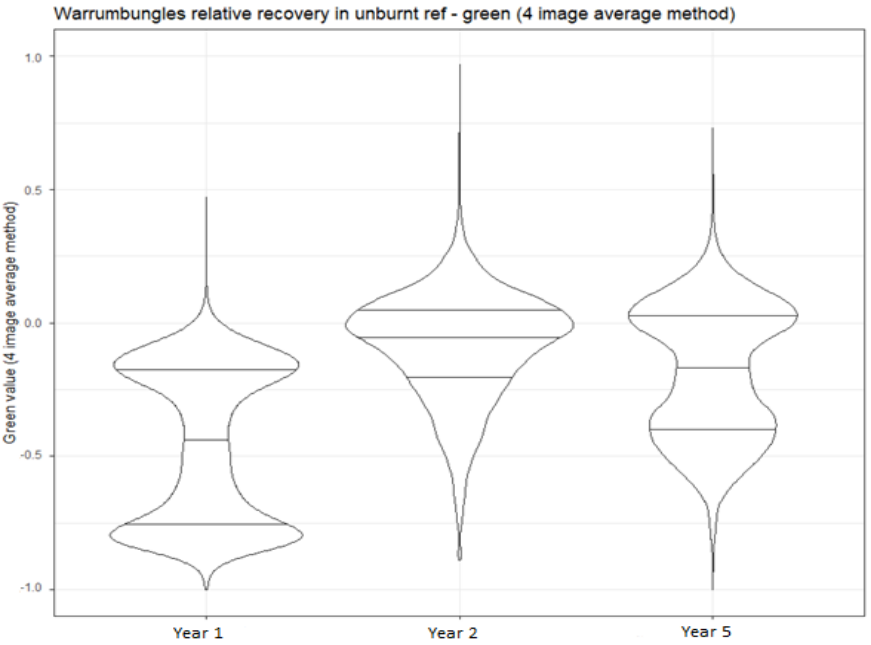

Figure 9 Relative recovery index for mean green fraction in the unburnt reference using 4 image average method

Further work will investigate possible refinements in better defining a representative unburnt reference location and the implications of different method options for applying a calibration correction. Validation against quantitative TLS field data will help to better understand the performance of different approaches. Further work will also target questions around the methodological implications of defining when a system is 'recovered' to either the pre-fire state or an alternative stable state.

5. Exploration of candidate radar recovery indices and techniques

Background

One of the aims of our project is to evaluate the use of radar derived indices for post-fire recovery monitoring. As a first step, we've used intensity differencing of pre- and post-fire Sentinel-1 data to test its performance in burnt area and fire severity mapping, using a random forest machine learning framework (i.e. the method used by FESM severity mapping). This will provide independent testing on quantified known measures of immediate post-fire effects on vegetation. This assessment will also have the benefit of scoping the potential for radar to be used in a rapid response severity mapping approach. As radar can penetrate cloud and smoke, this may help to overcome limitations of optical sensors, to potentially map fires progressively while they still burn, which was requested by DPIE executives of the FESM system during the extreme fire season of 2019/20.

The approach is being tested using Sentinel-1 C-band radar. C-band is a short wavelength (~5.6 cm) with limited penetration of dense vegetation canopies. Penetration depth depends on vegetation type and growth stage and is typically greater at longer wavelengths. Through our research networks, we are trying to secure access to longer wavelength L-band data (~24 cm wavelength) from the ALOS-2 PALSAR-2 so we can apply similar analyses.

The second step will be to determine the sensitivity of a radar time-series approach in detecting post-fire recovery for different fire severity classes and vegetation cover types. Time-series processing of monthly Sentinel-1 data acquired from January 2019 onwards is underway and exploratory metrics will be investigated in the next quarter. Batch processing is being implemented on DPIE's high performance computing system (SDC) for rapid processing of time-series data and integration with existing file storage and naming conventions.

Method

Pre- and post-fire intensity differencing

Sentinel-1 GRDH (ground range detected high resolution) data were acquired for 8 recent past wildfires (see Table 1, Gibson *et al* 2020). The data were orthorectified and radiometrically calibrated to gamma0 using ESA's SNAP v7.0 software. Pre- and post-fire images were differenced and clipped to the extent of each site. Input index values were extracted from API samples and for each severity class, which forms the training data for the supervised classification. Dr Michael Chang (Macquarie University) assisted in the analysis. The results for White Cedars and Pilliga fires are presented here.

Independent and combined fire severity models

Using a cross-validation framework with independent training and validation data, we have systematically compared multiple indices derived from optical, radar, and secondary texture indices across different pixel window sizes (**Table *7***). We also compared the integration of radar and optical data in combined models. Here we present the results for the White Cedars fire, which uses data from 7 other case study fires to train the models, tested against independent data from the target White Cedars fire.

Balanced accuracy statistics are reported, as well as overall accuracy and Kappa values, which determines the statistical agreement between the model and the validation data and allows comparative performance between models. For each model and the full model including all input indices, we calculated the mean decrease in Gini (Gini impurity criterion), which measures the similarity of a given element with respect to the rest of the classes and is used to find the best split

selection at each node of the random forest decision tree. The mean decrease in Gini was ordered from highest to lowest, to subsequently rank the input indices according to variable importance.

Results

Initial observations

Of the two polarizations, VH polarization appears more useful for detecting the burnt area and shows higher sensitivity to fire severity. VH backscatter is typically dominated by volume scattering between small vegetative components (leaves, twigs) in the upper canopy. Typically the magnitude of pre- and post-fire intensity difference at VH and VV polarizations increases as fire severity increases. Exceptions were observed at some sites (e.g., Tathra Wollemi) with similarly high mean VH intensity difference with fire severity class. Unburnt samples show limited change in intensity as expected.

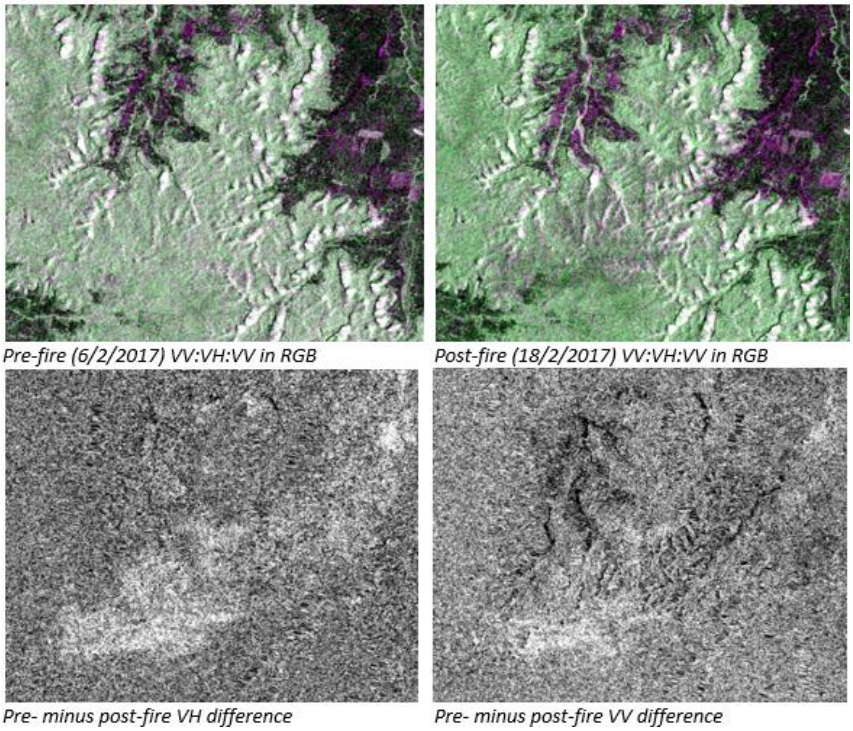

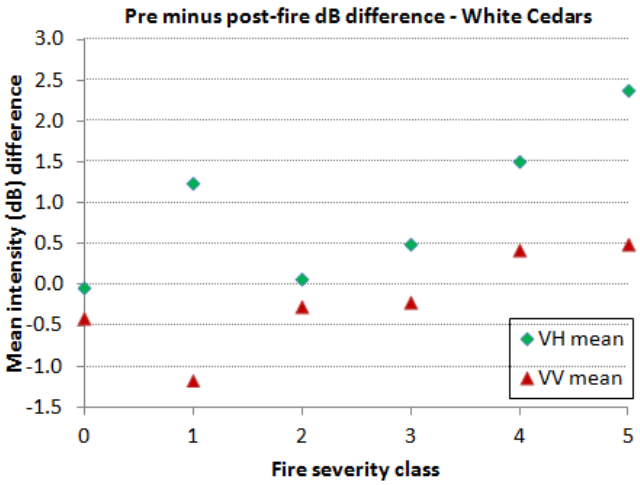

Figure 11 Sentinel-1A pre (6/2/2017) and post-fire (18/2/2017) gamm0 and pre-minus-post VH and VV intensity difference at White Cedars. Scatter plot of mean Sentinel-1 intensity difference for fire severity classes.

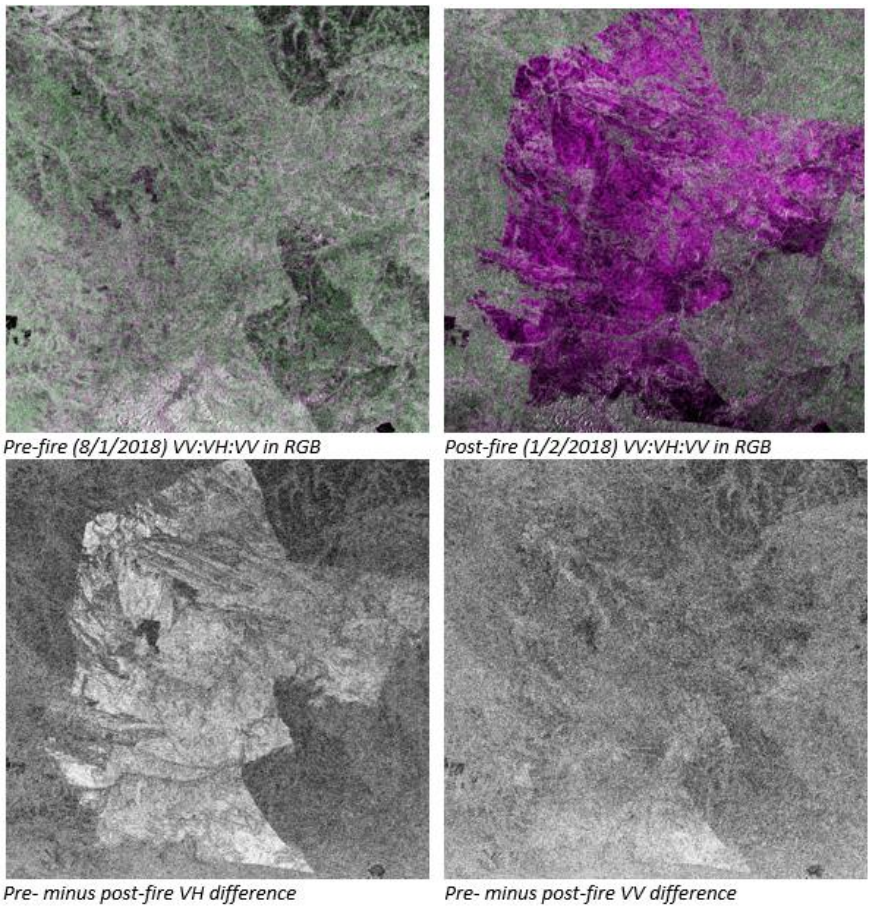

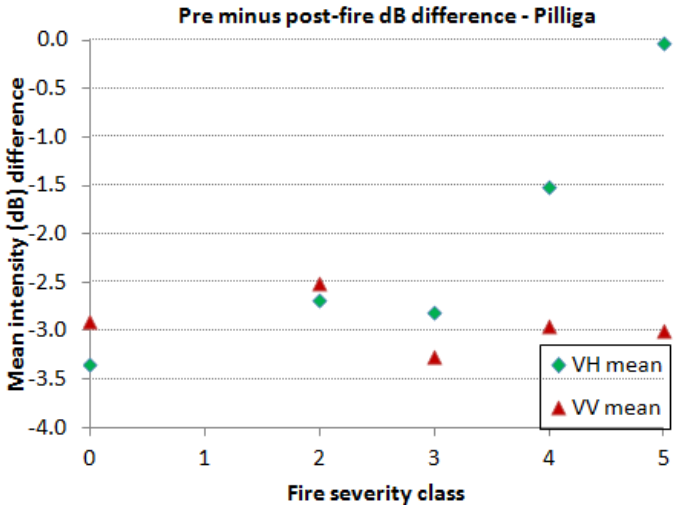

Figure 12 Sentinel-1A pre- (8/1/2018) and post-fire (1/2/2018) gamma0 and pre-minus-post VH and VV intensity difference at Pilliga. Scatter plot of mean Sentinel-1 intensity difference for fire severity classes.

Fire severity model performance

The results of the radar model indicate relatively poor performance in predicting severity classes, with 63% overall accuracy and 0.31 Kappa (**Table 8**). Kappa values <0.4 are considered to be poor. However, there was reasonable accuracy for the extreme severity class, with 85% balanced accuracy. When radar input indices were combined with SWIR derived indices, the model improved substantially, with 75% overall accuracy and 0.54 Kappa and an improved accuracy for high and extreme severity classes (79% and 98% respectively, Table 8). SWIR bands have been demonstrated in previous research to penetrate the atmospheric column even when aerosols such as smoke are present (but not cloud).

The optical model and the 'top 20 combined' model were very similar in performance metrics and included a similar set of input indices. However, the Radar – VH dissimilarity texture index (11 pixel window) was ranked 15 in variable importance in the full model, just 1 position lower than the very commonly used fire severity index, the dNBR (**Table 9**). Furthermore, several other Radar -VH derived texture indices (contrast, homogeneity and 2nd moment for 11-pixel windows) were ranked higher than the variance in dNBR (5-pixel window). Notably, the SWIR derived indices were consistently ranked higher than many of the other optical input indices that are used in the current FESM model, which provides significant insights towards improvements in future versions of FESM.

Initial comparisons of all 8 historic sites has revealed large differences in the sensitivity of pre-minus-post VV and VH polarizations to fire severity. Topography and rainfall may be influential factors on performance, as well as canopy openness. Understanding the reasons for these differences is the subject of ongoing work.

Table 7 Matrix of variables used in the comparison of models. The base index, texture statistic and pixel window size were combined to produce the input indices.

Sensor type	Base index	Texture statistic	Pixel window size
reflectance	dNBR	Mean (mean)	5
reflectance	RdNBR	Variance (var)	7
reflectance	SWIR dNBR2	Contrast (con)	11
reflectance	SWIR RdNBR2	2nd moment (2mom)	
fractional cover	Total cover	Homogeneity (hom)	
fractional cover	Bare cover	Dissimilarity (diss)	
radar	Radar - VV	Correlation (corr)	
radar	Radar - VH		

Table 8 Comparison of 4 models in the White Cedars cross-validation assessment, showing balanced accuracy statistics for each fire severity class, as well as the overall model accuracy and kappa statistics.

	Balanced Accuracy			
severity class	**top 20 combined**	**optical**	**radar**	**radar + swir**
unburnt	0.9639	0.9622	0.6883	0.7563
low	0.88686	0.88894	0.4997646	0.52783
mod	0.84304	0.83231	0.5000564	0.52775
high	0.90668	0.90899	0.501119	0.79729
extreme	0.9758	0.982	0.85269	0.9859
overall accuracy	0.9199	0.9192	0.6355	0.7525
Kappa	0.8698	0.8684	0.3061	0.5367

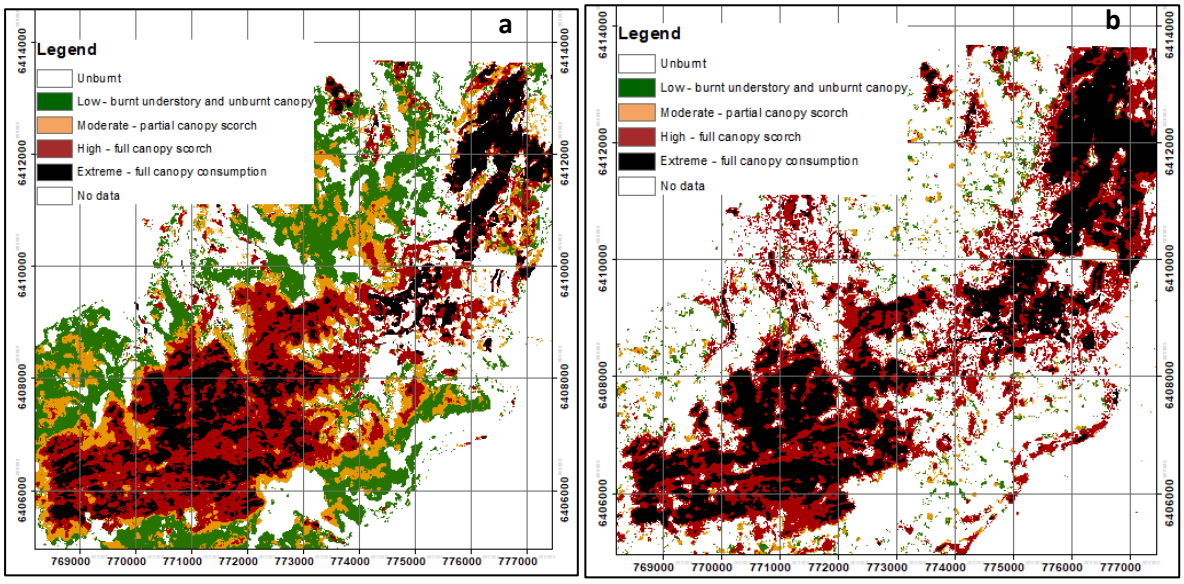

Figure 10 Visual comparison of optical (a) and radar + swir (b) models predicted severity class maps for the White Cedars fire

Table 9 Full list of input indices and the relative rank position for each model, based on the mean decrease in Gini index.

Input indices	full model	Optical only	Radar only	top radar + swir
mean_dBare7	1	2	NA	NA
RdNBR	2	1	NA	NA
mean_dBare5	3	5	NA	NA
glcm_SWIR_dNBR2_var_7	4	4	NA	1
SWIR_RdNBR2	5	6	NA	2
glcm_SWIR_dNBR2_mean_7	6	3	NA	3
glcm_SWIR_dNBR2_var_5	7	8	NA	4
glcm_SWIR_dNBR2_mean_5	8	7	NA	6
dBare	9	10	NA	NA
Rel_dTotal	10	11	NA	NA
mean_dNBR5	11	12	NA	NA
mean_dNBR7	12	13	NA	NA
SWIR_dNBR2	13	9	NA	5
dNBR	14	14	NA	NA
glcm_radarVH_dissim_11	15	NA	7	11
var_dBare7	16	15	NA	NA
glcm_radarVH_con_11	17	NA	5	8
glcm_radarVH_hom_11	18	NA	11	NA
glcm_radarVH_2mom_11	19	NA	6	9
var_dBare5	20	16	NA	NA
glcm_radarVH_var_11	21	NA	2	7
glcm_radarVV_con_11	22	NA	9	12
glcm_radarVH_mean_11	23	NA	3	10
glcm_radarVH_con_7	24	NA	17	NA
glcm_radarVV_dissim_11	25	NA	15	NA
glcm_radarVH_dissim_7	26	NA	22	NA
glcm_radarVV_mean_11	27	NA	1	14
glcm_radarVV_2mom_11	28	NA	16	NA
glcm_radarVV_var_11	29	NA	4	13
glcm_radarVV_hom_11	30	NA	19	NA
glcm_radarVH_mean_7	31	NA	13	NA
glcm_radarVH_var_7	32	NA	14	NA
glcm_radarVH_hom_7	33	NA	24	NA
var_dNBR5	34	18	NA	NA
var_dNBR7	35	17	NA	NA
glcm_SWIR_dNBR2_2mom_7	36	19	NA	NA
glcm_radarVV_mean_7	37	NA	10	15
glcm_radarVH_2mom_7	38	NA	23	NA
glcm_radarVV_var_7	39	NA	12	NA
glcm_SWIR_dNBR2_con_7	40	20	NA	NA
glcm_radarVV_con_7	41	NA	27	NA
glcm_SWIR_dNBR2_corr_7	42	21	NA	NA
glcm_SWIR_dNBR2_hom_7	43	22	NA	NA
glcm_radarVV_corr_11	44	NA	21	NA
glcm_radarVH_corr_11	45	NA	20	NA
glcm_SWIR_dNBR2_dissim_7	46	23	NA	NA
glcm_SWIR_dNBR2_corr_5	47	24	NA	NA
radar_inputVH	48	NA	18	NA
glcm_radarVH_corr_7	49	NA	25	NA
glcm_SWIR_dNBR2_2mom_5	50	25	NA	NA
radar_inputVV	51	NA	8	16

Input indices	Combined model	Optical only	Radar only	top radar + swir
glcm_radarVV_corr_7	52	NA	26	NA
glcm_radarVV_dissim_7	53	NA	31	NA
glcm_radarVV_2mom_7	54	NA	30	NA
glcm_radarVV_hom_7	55	NA	28	NA
glcm_SWIR_dNBR2_con_5	56	27	NA	NA
random	57	26	29	17
glcm_SWIR_dNBR2_hom_5	58	28	NA	NA
glcm_SWIR_dNBR2_dissim_5	59	29	NA	NA

6. Field Data

Terrestrial Laser Scanner

A TLS is an active ground-based system for rapid collection of 3D point clouds of objects. The TLS emits laser pulses towards its target and measures the distance from the device to the target. The intensity of the return pulse is also recorded. With TLS we can reconstruct the three-dimensional forest canopy and assess vegetation dynamics post-fire. The TLS provides rapid and objective assessment of forest structure and can be repeated at appropriate time intervals.

Significant investment of our time in the past few months since acquiring the TLS has been focused on technical training and developing protocols to allow for high precision repeat site surveys, data management and automating workflows for file naming conventions, data storage, pre- and post-processing and analysis. We have leveraged significant in-house expertise through our JRSRP research partner Dr Nick Goodwin, to implement much of the previously scripted workflows Nick and colleagues had developed in QLD (Department of Environment and Science). Ongoing development and testing are still taking place to further refine processing efficiencies and data analysis output.

TLS field capture method

Our standard TLS field method involves the following key components:

- A single TLS site is comprised of 7 scan positions, with one central scan and 6 scans located at 33m from the central scan in a star transect configuration (N, NE, SE, S, SW, NW). The 7 scan positions are co-registered during processing.
- Each of the scan positions is comprised of 2 x 360-degree scans (horizontal and vertical), which are co-registered as a pre-processing step.
- To support high precision site revisit data, an underground steel recovery is positioned at each scan position and recovered using a metal detector.

For the post-fire recovery project, 2 TLS sites are paired, with an unburnt (or low severity) site and a high (or extreme) severity location in the most recent past fire. The paired sites are assessed as closely comparable in terms of proximity, pre-fire canopy height and density and topographic position, estimated from pre-fire LiDAR wherever possible. The pairing of sites will be critical to provide the unburnt/lower severity reference for relative comparison of the post-fire recovery rates.

Preliminary TLS data analysis

Here we present example TLS images and metrics from our 4 test sites. We surveyed 1 site twice to examine our revisit accuracy and precision (200722_060219 and 200722_065623). These test sites won't be included in ongoing monitoring as we have further refined our methods for paired site selection and repeat capture precision. Using the TLS data from our 4 test site locations, post-processing analysis using the pylidar python library generated statistics of the diameter at breast height (DBH 1.3m) and number of stems (**Table *10***), plus total cover and total wood volume (**Table *11***). Total cover is defined as the fraction of the ground covered by 2D gridded return heights greater than 2m, using a grid resolution of 5cm. Volume metrics are computed within 5cm vertical intervals with an estimate of diameter for each interval. Visualisation of the maximum height above ground (max HAG) for each site is provided in **Figure *11***. We generated modelled output including estimated mean DBH as a function of height (**Figure *12***), estimated number of stems/branches as a function of height (**Figure *13***), and estimated stem/branch volume as a function of height (**Figure *14***). Further work is currently being undertaken to incorporate statistics of cover as a function of height (i.e. canopy height profiles) in our data analysis workflows.

Table 10 TLS Site statistics, including DBH measures and number of stems.

	DBH 1.3m				
Site name	max	mean	median	sd	number of stems
200722_060219*	0.938	0.114	0.095	0.059	1042
200722_065623*	0.938	0.113	0.094	0.066	1038
200723_015553	0.844	0.101	0.078	0.064	1371
200722_011909	0.883	0.131	0.094	0.093	888

Table 11 TLS Site statistics, including total cover and total wood volume.

Site	Total Cover (>2m)	Total wood volume (m3)
200722_060219*	0.604	163.258
200722_065623*	0.604	163.104
200723_015553	0.892	333.968
200722_011909	0.824	286.365

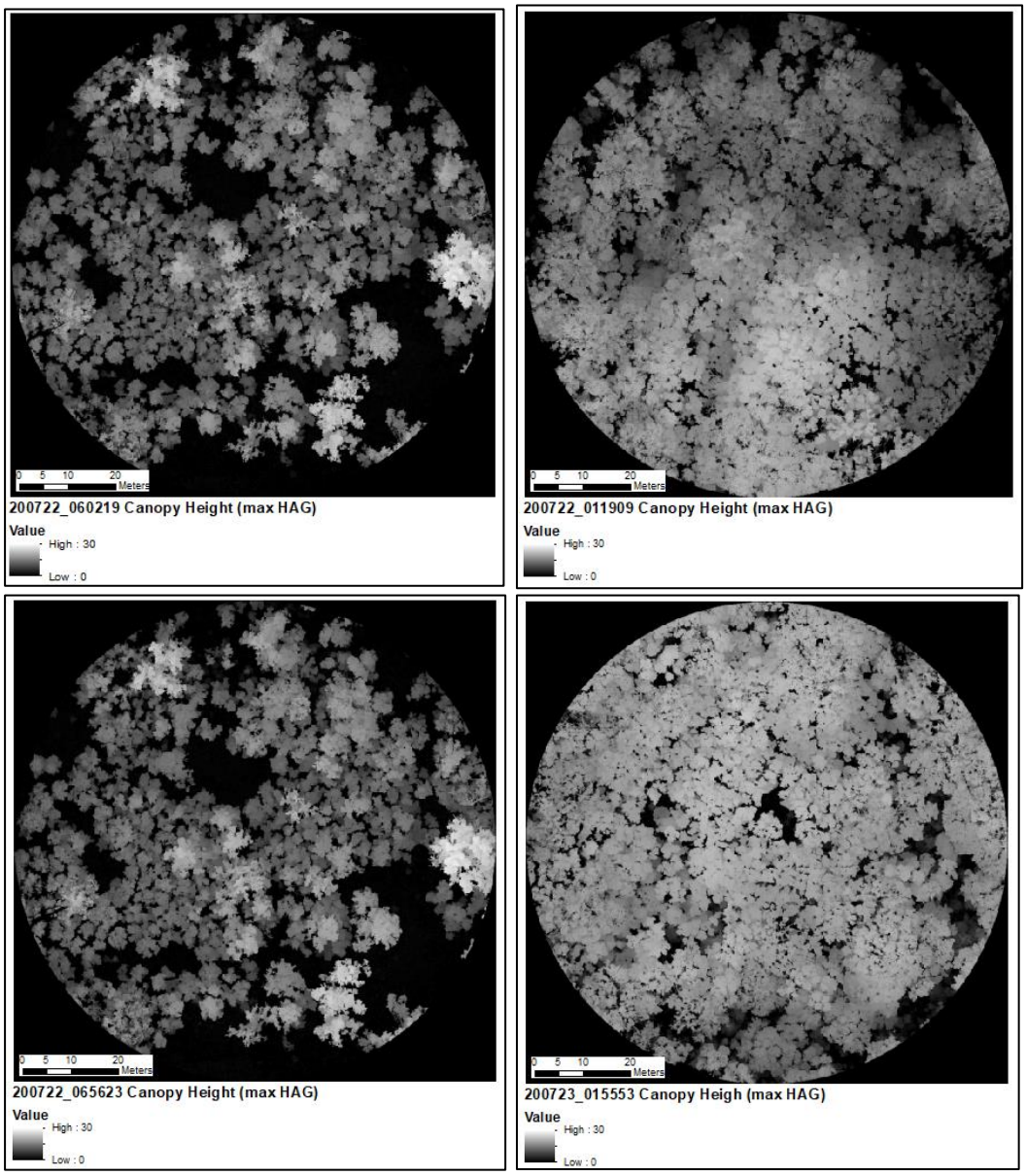

Figure 11 Canopy Height imagery for each TLS site

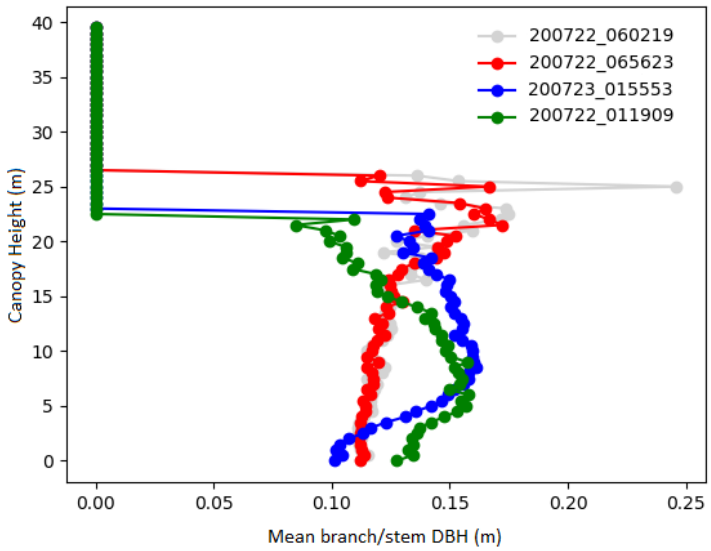

Figure 12 estimated mean DBH as a function of height for each TLS site.

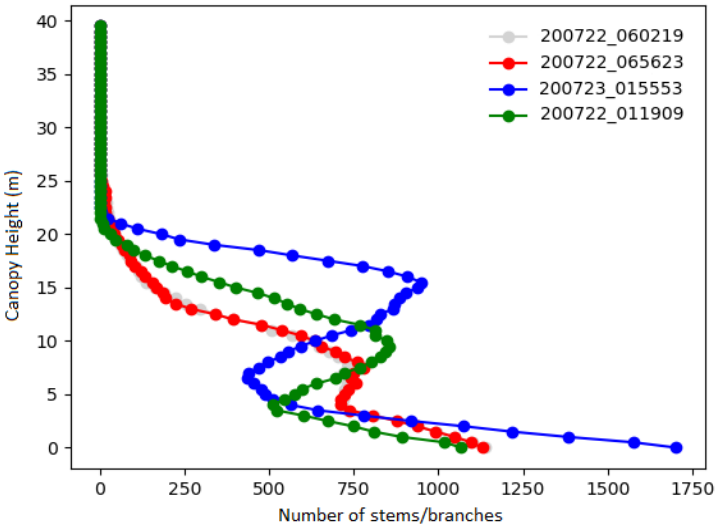

Figure 13 estimated number of stems/branches as a function of height for each TLS site.

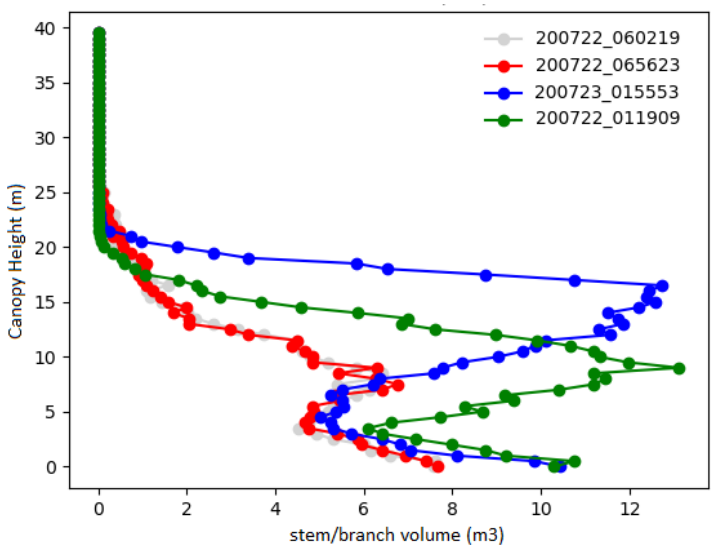

Figure 14 estimated stem branch volume as a function of height for each TLS site.

Post-fire recovery TLS site locations for repeat surveys

Site selection has focused on the northern half of NSW to restrict personnel movement during the the COVID pandemic. We have commenced setting up permanent TLS post-fire recovery monitoring sites (**Table *12*** and **Figure *15***), with 2 clusters of paired sites (i.e. 4 sites) in Clouds Creek State Forest in the 2019/20 Liberation Trail fire. Our sites in the Shark Creek fire in Yuragir NP have been located with site reconnaissance but fieldwork was postponed due to rain. Similarly, fieldwork for the Bees Nest fire in Guy Fawkes River NP was scheduled for the 27-28th October but was postponed due to rain. Sites in the 3 fires out west in the Pilliga and Mt Kaputar NP will be captured during fieldwork scheduled for 3rd – 7th November, with the Mt Nardi sites planned to be captured in mid-November. Additional single-visit sites with longer time since fire may be opportunistically captured during our site re-visit field trips.

Several of these TLS sites have been selected due to overlapping objectives with collaborative research partners, including Anthea Mitchell's ALOS regrowth mapping out in the Pilliga, Grant Hodgins Old Growth Mapping in Clouds Creek SF, and Mitch Lyons, David Keith and Rob Kooyman's threatened species post-fire recovery work in lowland rainforest in Mt Nardi.

Table 12 Permanent TLS post-fire recovery monitoring site location details

Fire name	Fire start date	Fire End date	Location	Cluster	Site name	x coord.	y coord.	Fire Severity
Liberation Trail	4/11/2019	24/12/2019	Clouds Creek SF	1	200923_122611	465489.580	6667229.070	unburnt/low
				1	200923_154324	465675.300	6666973.640	high/extreme
				2	200924_102321	465560.840	6674291.850	unburnt/low
				2	200924_130236	465791.160	6673915.990	high/extreme
Shark Creek	13/08/2019	12/10/2019	Yuragir NP	3	TBC	TBC	TBC	unburnt/low
				3	TBC	TBC	TBC	high/extreme
Bees Nest	31/08/2019	13/11/2019	Guy Fawkes River NP	4	TBC	TBC	TBC	unburnt/low
				4	TBC	TBC	TBC	high/extreme
Mt Nardi	8/11/2019	29/11/2019	Nightcap NP	5	TBC	TBC	TBC	unburnt/low
				5	TBC	TBC	TBC	high/extreme
Kerringle	29/11/2006	9/01/2007	Pilliga East CR	6	TBC	TBC	TBC	unburnt/low
				6	TBC	TBC	TBC	high/extreme
Dipper Rd	17/01/2018	2/02/2018	Pilliga NR	7	TBC	TBC	TBC	unburnt/low
				7	TBC	TBC	TBC	high/extreme
Mt Kaputar	17/10/2019	4/12/2019	Mt Kaputar NP	8	TBC	TBC	TBC	unburnt/low
				8	TBC	TBC	TBC	high/extreme

Figure 15 Permanent TLS post-fire recovery monitoring site locations

7. Risk/vulnerability modelling

Satellite time series can be used to track forest recovery over time. Conceptually, this approach involves determining when the satellite signal returns to its pre-disturbed level. For optical systems like Landsat, this recovery indicator is considered 'spectral' recovery, as opposed to structural or compositional recovery. However, spectral recovery has been shown to correlate with structural recovery and can act as a reasonable proxy for monitoring forest recovery, particularly at the landscape scale. Recent research undertaken in Victoria found that spectral recovery length was often more strongly influenced by environmental factors rather than the severity of the fire (Hislop et al. 2019).

This sub-task is based on the premise that information about spectral recovery from past fires can be harnessed to 'predict' future recovery durations, based on knowledge about vegetation type, location, fire severity, etc. Initial exploratory analysis of spectral recovery following past fires in NSW indicate substantial differences across bioregions (Figure XX). This analysis is based on human interpreted reference samples (~1000 randomly assigned 1 hectare patches). Moving forward, the aim of this task is to generate predicted maps of recovery duration over the 2019-2020 fire extent. This will help to identify vulnerable areas where management interventions may be most beneficial.

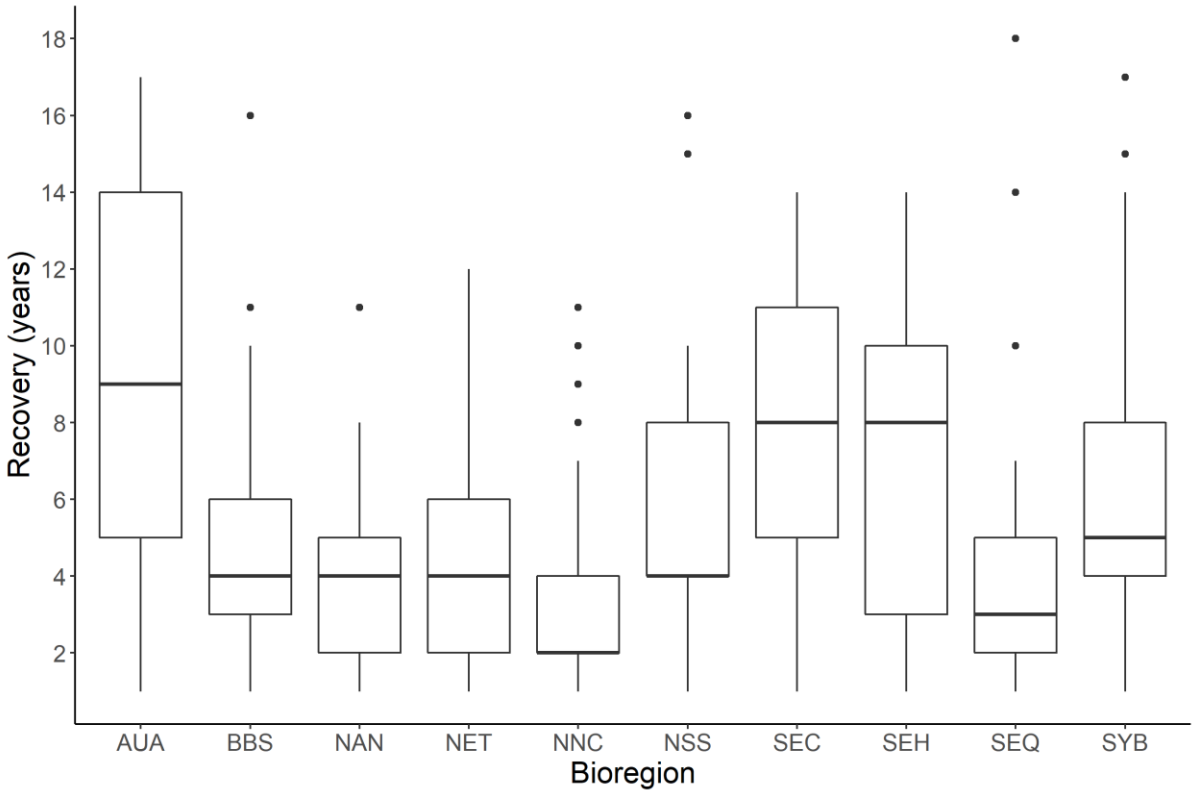

Figure XX. Boxplots of spectral recovery length in NSW eastern bioregions, as determined by human interpretation of Landsat data samples.

8. Next tasks

The following section summarises the key tasks we will be focusing on over the next 6 months.

Fire Severity Derived post-fire ecological recovery decision support tools

- Continue building the Blue Mountains Case Study
- minor data quality refinements and reprocess finalised file formats of the fire year mosaics, fire frequency and TSF products
- generate products to enhance the ecological context by intersect unburnt canopy products with vegetation formation and topographic position (i.e. ridge, gully, slope)
- re-running the landscape pattern statistical analyses.
- investigate quantitative evidence and further understanding of the effect of unburnt canopy patchiness on ecological resilience.

Optical sensor analysis

- Further explore candidate spectral and fractional cover indices across a wider range of vegetation, climate and topographic conditions,
- Investigate possible refinements in defining a representative unburnt reference
- Test different method options for applying a calibration correction.
- Validation of indices against quantitative TLS field data
- Examine methodological implications of defining when a system is 'recovered' to either the pre-fire state or an alternative stable state.

Radar sensor analysis

- Co-registration and final processing of monthly sentinel-1 time-series and exploration of time-series metrics for post-fire recovery
- Run remaining fire severity models using radar-only, optical-only and combined inputs and identify strengths and limitations of each approach
- Explore potential of dense time-series (weekly) of sentinel-1 for rapid response mapping of burnt area extent

TLS field data

- Continue setting up permanent TLS monitoring sites
- Refine post-processing data analysis scripted workflow
- Conduct preliminary analysis of TLS field data comparisons to satellite-derived relative recovery products.

Predictive post-fire recovery risk modelling

- Continue building the reference sample database
- preliminary analysis to generate predictive maps of recovery duration over the 2019-2020 fire extent

References

Gibson, R., Danaher, T., Hehir, W. and Collins, L. (2020) 'A remote sensing approach to mapping fire severity in south-eastern Australia using sentinel 2 and random forest', *Remote Sensing of Environment,* 240(111702).

Hislop, S., Jones, S., Soto-Berelov, M., Skidmore, A., Haywood, A. and Nguyen, T. H. (2018) 'Using Landsat spectral indices in time-series to assess wildfire disturbance and recovery', *Remote sensing,* 10(460).

Hislop, S., Jones, S., Soto-Berelov, M., Skidmore, A., Haywood, A., Nguyen, T.H. (2019). High fire disturbance in forests leads to longer recovery but varies by forest type. Remote Sens. Ecol. Conserv. 1–13. https://doi.org/10.1002/rse2.113

Appendix 1

FESM Sentinel 2 vs Landsat 8 algorithm comparison

Table 13 ***Balanced Accuracy and Kappa statistics for predictive models for each fire.***

	FESM class	**FESMv2 Sen2**	**FESMv2 L8**
Tathra	unburnt	0.967	0.970
	low	0.845	0.945
	moderate	0.726	0.771
	high	0.842	0.816
	extreme	0.972	0.854
	Kappa	0.693	0.711
Holsworthy	unburnt	0.985	0.992
	low	0.798	0.939
	moderate	0.729	0.576
	high	0.763	0.815
	extreme	0.939	0.925
	Kappa	0.6872	0.756
Mt Canobolas	unburnt	0.944	0.958
	low	0.872	0.883
	moderate	0.612	0.748
	high	0.933	0.758
	extreme	0.937	0.866
	Kappa	0.717	0.698
Pilliga	unburnt	0.998	0.988
	low	0.804	0.877
	moderate	0.592	0.639
	high	0.774	0.902
	extreme	0.605	0.964
	Kappa	0.539	0.891

	FESM class	FESMv2 Sen2	FESMv2 L8
Sir Bertram	unburnt	0.995	0.994
	low	0.825	0.958
	moderate	0.538	0.884
	high	0.748	0.745
	extreme	0.983	0.711
	Kappa	0.744	0.538
Sir Ivan	unburnt	0.945	0.885
	low	0.729	0.662
	moderate	0.671	0.609
	high	0.804	0.644
	extreme	0.958	0.954
	Kappa	0.765	0.663
White Cedars	unburnt	0.979	0.996
	low	0.908	0.949
	moderate	0.726	0.756
	high	0.915	0.916
	extreme	0.933	0.960
	Kappa	0.832	0.857
Wollemi695	unburnt	0.989	0.973
	low	0.831	0.739
	moderate	0.648	0.7682
	high	0.906	0.835
	extreme	0.950	0.925
	Kappa	0.767	0.657